Rheology of wet granular materials under continuous shear: experiments and simulations

Michel Badetti[1,⋆], *Abdoulaye* Fall[1,⋆⋆], and *Jean-Noël* Roux[1,⋆⋆⋆]

[1] *Laboratoire Navier, UMR8205, CNRS-ENPC-IFSTTAR,2 allée Kepler, 77420, Champs-sur-Marne, France*

Abstract. The behaviour of wet granular media in shear flow is characterized by the dependence of apparent friction μ^* and solid fraction Φ_S on the reduced pressure P^* and the inertia number I. Reduced pressure, $P^* = \sigma_{22}a^2/F_0$, compares the applied normal stress σ_{22} on grains of diameter a to the tensile strength of contact F_0 (proportional to the surface tension Γ of the liquid and the beads diameter). A specifically modified rotational rheometer is used to characterize the response of model wet granular material to applied shear rate $\dot{\gamma}$ under controlled normal stress σ_{22}. Discrete Element Method (DEM) simulations in 3D are carried out in parallel and numerical results are compared with experimental ones. Cohesive, inertia, saturation and viscous effects on macroscopic coefficient of friction μ^* and solid fraction Φ_S are discussed.

1 Introduction

In the steady state, shear flows of granular materials under controlled normal stress σ_{22} and shear rate $\dot{\gamma}$ (see Fig. 1) are well described by the solid fraction Φ_S and the macroscopic friction coefficient $\mu^* = \sigma_{12}/\sigma_{22}$. Characterizing flow inertia of such materials with the inertial number $I = \dot{\gamma}a\sqrt{m/a\sigma_{22}}$ (m being the mass of a grain and a its diameter) is now a classical approach [1, 2]. However, recent studies showed that in the case of wet granular materials there is also a strong dependency of both μ^* and Φ_S on the cohesive effect induced by liquid bonding between particles [3–5]. For a pack of beads of diameter a with bonds strength f_0, the reduced pressure $P^* = a^2\sigma_{22}/f_0$ can characterize this cohesive effect.

Previous DEM studies proposed constitutive laws $\mu^*(I, P^*)$ and $\Phi_S(I, P^*)$ covering broad ranges of I and P^* [3]. The aim of the present commuication is to compare these DEM simulations of wet grain assemblies with new experimental measurements using a normal stress controlled shear cell, both in the quasistatic limit and in dense inertial flows.

Sec. 2 describes the model material and the shearing methods. Sec. 3.1 compares flow curves of our materials obtained numerically and experimentally, in Sec. 3.4 and 3.5 respectively the influence of liquid volume Φ_L and viscosity η in the quasistatic regime is discussed.

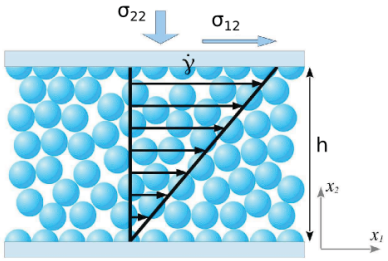

Figure 1. Ideal plane shear with confinement. shear rate is defined as $\dot{\gamma} = \partial\dot{x}_1/\partial x_2$.

2 Methods

2.1 Model material

In simulations and experiments, the model material proposed is a simple pack of monodisperse spherical polystyrene beads of diameter $a = 5 \times 10^{-4}$m mixed together with a newtonian silicon oil of surface tension $\Gamma = 47$mN.m^{-1} and variable viscosity η ranging from 20mPa.s up to 1000mPa.s. Liquid quantity is described by the ratio Φ_L/Φ_S which ranges from 0.003 up to 0.075 [6–8], thus ensuring a pendular state. In such state, for a perfecting wetting fluid bond strength at contact f_0 is well approximated by $\pi a\Gamma = 7.38 \times 10^{-5}$N [9].

⋆e-mail: michel.badetti@ifsttar.fr
⋆⋆e-mail: abdoulaye.fall@ifsttar.fr
⋆⋆⋆e-mail: jean-noel.roux@ifsttar.fr

2.2 Experimental setup

Materials are inserted in a specifically devised rheological cell (see Fig. 2). Constant force F_N and rotation rate w are applied on a volume V_S of material, Torque T and material width h (see Fig. 1) are measured once plateau values of the steady state are reached. Assuming plane shear with truncated center, σ_{12}, σ_{22}, $\dot{\gamma}$ and Φ_S are calculated as :

$$\sigma_{12} = \frac{3T}{2\pi R_e^3 \left(1-(R_i/R_e)^3\right)}$$

$$\sigma_{22} = \frac{F_N}{\pi R_e^2 \left(1-(R_i/R_e)^2\right)}$$

$$\dot{\gamma} = w\frac{R_e+R_i}{2h}$$

$$\Phi_S = \frac{V_S}{\pi h R_e^2 \left(1-(R_i/R_e)^2\right)}$$

Materials are inserted to ensure a width $h > 20a$, the gap between inner R_i and outer radii R_e is equal to $20a$. Experimental measures with different values of h (see figure 3 showed no gap effect ruling out possibilities of localization effects. Similar devices have already been used to describe succesfully the rheology of dense suspensions and dry materials [1, 2, 10]. Means and error bars are obtained for materials tested at least 3 times.

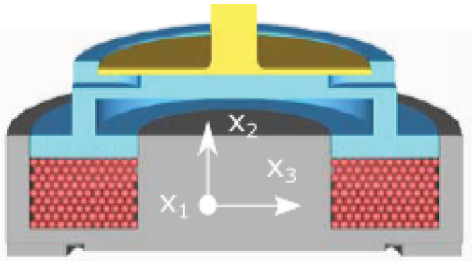

Figure 2. Rheological cell : gains (red) are trapped between the stator (grey) and the rotor (blue+yellow). Shear happens in the $\mathbf{x_1}$,$\mathbf{x_2}$ plane. Outer and inner radii are respectively R_e and R_i

2.3 Numerical simulations

Materials are placed in a 3D periodical cell sheared using Lees-Edwards boundary conditions. Shear rate $\dot{\gamma}$ and σ_{22} are applied, σ_{12} and Φ_S are measured. Contact interaction are implemented using an Hertz-Mindlin model with viscous dissipation, friction in contact satisfies Coulomb's law with a friction coefficient $\mu = 0.09$ chosen in order to fit values of $\mu^* = \mu_d^* = 0.257$ and $\Phi_S = \Phi_{S,d} = 0.616$ for $I \to 0$ and $P^* \to \infty$ found experimentally (see figure 4). Distant interactions involve meniscii assumed to form only when grain come into contact with a fixed volume V_m, they disappear at a certain rupture distance $D_0 = V_m^{1/3}$. Error bars are obtained using the technique of block transform estimates [11].

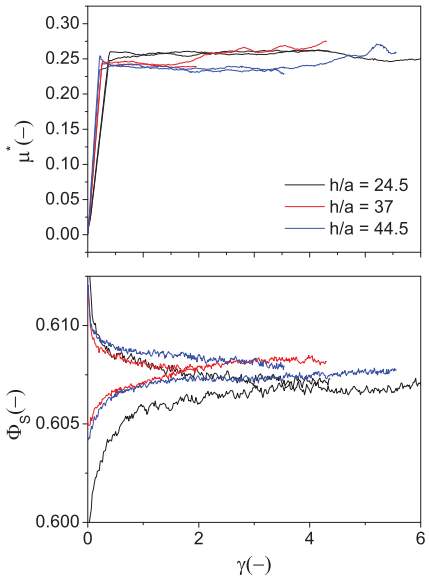

Figure 3. μ^* and Φ_S measured at different sample width. Absence of gap effect is highlighted. Measurements made with $\eta = 20$mPa.s, $\Phi_L/\Phi_S = 0.075$, $I = 10^{-4}$ and $P^* = 3$

3 Results

3.1 Inertia and cohesive effects

Figure 4 presents μ^* and Φ_S as functions of I for different values of P^* in experiments and simulations. For low values of I ($< 10^{-3}$), ie in the quasistatic regime, μ^* and Φ_S reach plateau values. For higher values of I, in the inertial regime, μ^* increases and Φ_S decreases upon increasing I.

Table 1 compares experimental and numerical data when $I = 10^{-3}$, values recorded with the two methods show very good agreements with less than 6% relative difference for μ^* and less than 3% relative difference for Φ_S.

The agreement between simulations and experiments remains good when comparing the solid fractions for inertial flows, the maximal relative difference between experiments and simulations is at most 0.5% for $P^* = 2$ and 0.8% for $P^* = 3$. There is, however, a discrepancy when looking at the values of μ^* in the inertial regime. When $I > 3 \cdot 10^{-3}$, the relative difference rises up to 30% for P*=3 and up to 17% for P*=2. Clearly, μ^* increases much faster with I away from its quasistatic value μ_0^* for $I \to 0$ in the experiments than in the numerical simulations. This discrepancy could emerge from questions of liquid repartition in the experimental samples.

Table 1. Values of μ_0^* and Φ_S obtained for $I < 10^{-3}$, $\Phi_L/\Phi_S = 0.03$ and $\eta = 550$mPa.s. exp and num subscripts respectively stand for experimental and numerical

P^*	μ^*_{exp}	μ^*_{num}	$\Phi_{S,exp}$	$\Phi_{S,num}$
∞	0.255	0.257	0.616	0.616
3	0.302	0.327	0.606	0.605
2	0.340	0.364	0.595	0.597

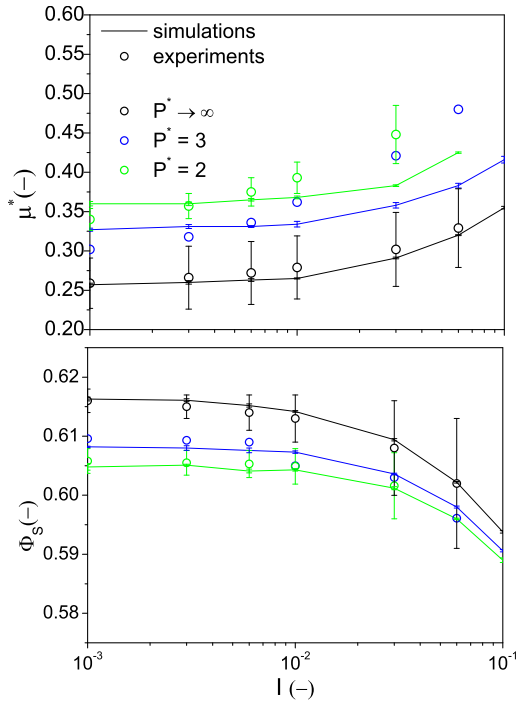

Figure 4. Flow curves $\mu^*(I, P^*)$ and $\Phi_S(I, P^*)$. filled circles represent experimental data while lines representnumerical data. Dry samples in black, $P^* = 3$ in blue and $P^* = 2$ in green. For wet samples viscosity $\eta = 550$mPa.s and $\Phi_L/\Phi_S = 0.015$.

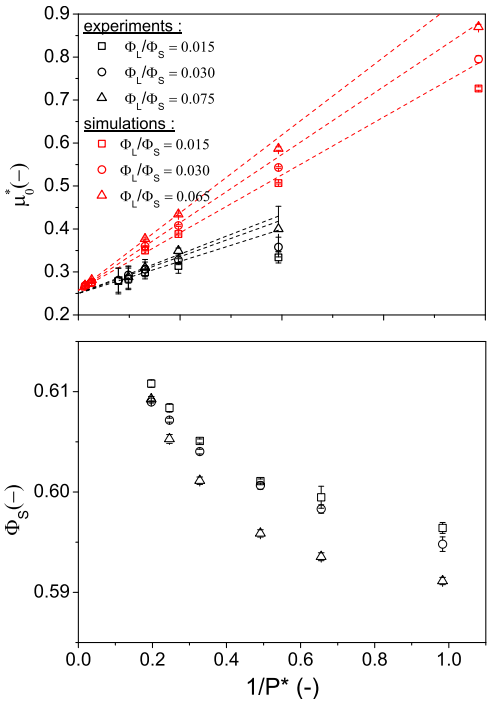

Figure 5. Numerical (open symbols) and experimental (filled symbols) values of μ_0^* and Φ_S versus $1/P^*$ for different values of Φ_L/Φ_S, $\eta = 550$mPa.s. Linear approximation of μ_0^* from equation 2 given in dashed lines.

3.2 Quasistatic regime : Saturation effect

Fig. 5 shows numerical and experimental μ_0^* versus $1/P^*$ for different ratio Φ_L/Φ_S. For poorly cohesive materials ($1/P^* = 0.033$), numerically increasing Φ_L/Φ_S from 0.015 up to 0.06, μ_0^* grows by 1%. For highly cohesive ones ($1/P^* = 1$), increasing Φ_L/Φ_S from 0.015 up to 0.075 experimentally and from 0.015 up to 0.06, μ_0^* grows by 16%. On the whole range of $1/P^*$, Fig. 5 also shows that Φ_S barely depends on Φ_L/Φ_S.

Assuming the quasistatic behavior of wet granular materials can be expressed through a Mohr-Coulomb criterion, e.g materials flow with :

$$\sigma_{12} = \mu_d^* \sigma_{22} + C \tag{1}$$

where cohesion C is defined as a rupture tangential stress in unconfined conditions. Ensuring $\sigma_{22} = 0$Pa is not possible with the methods at our disposal. However, knowing the constant macroscopic coefficient of friction μ_d^* of dry granular material, C can be estimated at various σ_{22}. Using equation 1, numerical estimation are averaged for $\sigma_{22} = 9000$Pa and 4500Pa, experimental ones are averaged for $\sigma_{22} = 1500$Pa and 1200Pa, the values obtained are reported in table 2. Estimates of C increase up to 39% within the range of Φ_L/Φ_S. Noting that Eq. 1 is equivalent to :

$$\mu_0^* = \mu_d^* + \frac{a^2 C}{f_o} \frac{1}{P^*} \tag{2}$$

one expects a linear evolution of μ_0^* with $1/P^*$, with a slope proportional to C and the constant ratio a^2/f_0. Fig. 5 exhibit linear predictions of μ_0^* with the values of cohesion given in Table 2, those predictions remain good with less than 5% relative difference with actual measurements when $1/P^* < 1$.

Assuming capillary forces introduce negligible contribution to shear stress, cohesion in granular media can also be approximated theoretically [3, 4] as :

$$C = \mu_d^* \frac{f_0}{a^2} \frac{\Phi_S z}{\pi} \tag{3}$$

In the whole range of $1/P^*$, the simulations show that the variations of the product $\Phi_S z$ are small (10% at most), while the cohesion estimated from equation 1 can vary up to 30% in simulations and up to 40% in experiments . It is likely that neglecting the contribution of capillary forces to shear stress, when the cohesive effect is high $1/P^* > 1$, is too strong an assumption.

Table 2. Values of cohesion C in Pa. As deduced from experiments (C_{exp}), simulations (C_{num}) and approximation (eq. 3, C_{app}).

Φ_L/Φ_S	C_{exp}	C_{num}	C_{app}
0.003		76.7	91.2
0.007		77.2	93
0.015	42	77.4	95.2
0.030	49	94.7	97.5
0.060		108.2	100
0.075	50	126.2	103.8

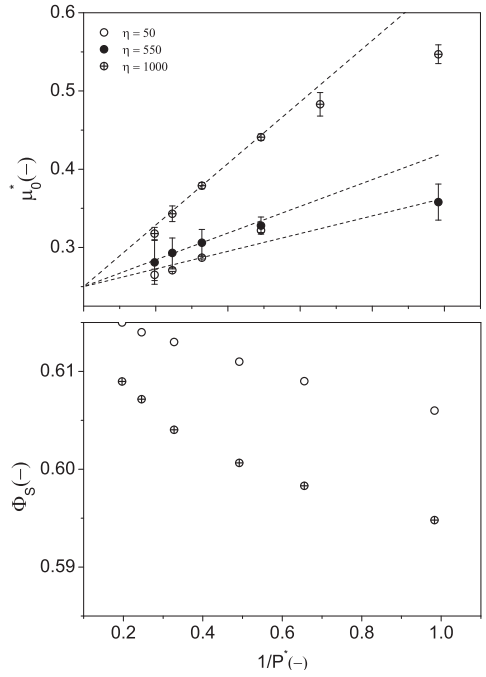

Figure 6. experimental values of μ_0^* and Φ_S versus $1/P^*$ for different values of η, $\Phi_L/\Phi_S = 0.03$. Linear approximations of μ_0^* from equation 2 are given by the dasehd lines.

3.3 Quasistatic regime : Viscosity effect

Fig. 6 shows the experimental value of μ_0^* and Φ_S versus $1/P^*$ for different values of viscosity η. As remarked above (Sec. 3.2), the linear variation of μ_0^* with $1/P^*$ shows the applicability of a Mohr-Coulomb criterion of plastic flow for $1/P^* < 1$.

Identified cohesion values appear to vary with the viscosity of the liquid, ranging from 33Pa for $\eta = 50$mPa.s up to 116Pa for $\eta = 1000$mPa.s. A strong influence of the viscosity on friction coefficient μ_0^* is also observed in the cohesion dominated regime, when $1/P^* > 1$. Solid fraction Φ_S, on the other hand, is not sensitive to η variations. While viscous forces through liquid bridges are negligible at low velocities [9], one may speculate that a higher viscosity affects the rate with which liquid is transported between different meniscii in the contact network, leading to more heterogeneous liquid distributions. In turn, such heterogeneities, possibly involving complex structures merging independent meniscii together (as apparent in Fig. 7, obtained by X-ray microtomography on one of the experimental samples) could explain the unexpected increase of μ_0^* with η.

Conclusion

While the effects of I,P^* and Φ_L/Φ_S, which are observed in the simulations are satisfactorily understood, the unexpected influence of the liquid viscosity could be attributed to inhomogeneous distributions of the liquid content in the sheared sample. Such inhomogeneities might affect the rheological properties (and possibly explain the stronger I dependence of experimental data, compared to numerical ones). More systematic microstructural studies using X-ray microtomography are planned to investigate these effects.

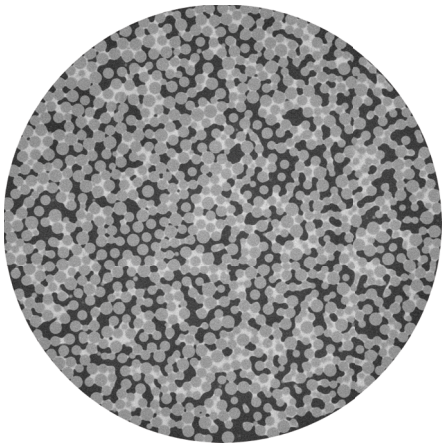

Figure 7. Microtomography image : slice of a sample, $\Phi_L/\Phi_S = 0.075$ and $\eta = 1000$mPa.s.

References

[1] A. Fall, G. Ovarlez, D. Hautemayou, C. Mézière, J.-N Roux, F. Chevoir, J. of Rheol. **59**, 2015
[2] A. Fall, M. Badetti, G. Ovarlez, F. Chevoir, J.-N Roux, *these proceedings*, 2016
[3] S. Khamseh, J.-N. Roux, F. Chevoir, Phys. Rev. E **92**, 2015
[4] V. Richefeu, M.S. El Youssoufi, F. Radjaï, Phys. Rev. E **73**, 2006
[5] F.A. Gilabert, J.-N. Roux, A. Castellanos, Phys. Rev. E**75**
[6] M. Scheel, R. Seemann, M. Brinkmann, M. Di Michiel, A. Sheppard, S. Herminghaus, J.of Phys.:Cond.Matt **20**, 2008
[7] N. Mitarai, F. Nori, J.of Phys.:Cond.Matt, 2006
[8] P.C.F. Moller, D. Bonn, EuroPhys. Letters **80**, 2008
[9] O. Pitois, P. Moucheront, C; Chateau, J. Coll. Interf. Science **231**, 2000
[10] F. Boyer, E. Guazzelli, O. Pouliquen, Phys. Rev. Letter **107**, 2011
[11] H. Flyvbjerg, H. G. Petersen, J. Chem. Phys. **91**, 1989